molecular pharmaceutics

ARTICLE

pubs.acs.org/molecularpharmaceutics

Time-Resolved SAXS/WAXS Study of the Phase Behavior and Microstructural Evolution of Drug/PEG Solid Dispersions

Qing Zhu,[†] Michael T. Harris,[†] and Lynne S. Taylor*[,‡]

[†]School of Chemical Engineering and [‡]Department of Industrial and Physical Pharmacy, Purdue University, West Lafayette, Indiana 47907, United States

Supporting Information

ABSTRACT: Simultaneous small-angle X-ray scattering/wide-angle X-ray scattering (SAXS/WAXS) was employed to elucidate the physical state and location of various small molecule drugs blended with polyethylene glycol (PEG), as well as the time dependent microstructural evolution of the systems. Samples were prepared by comelting physical mixtures of the drug and PEG, followed by solidification at 25 °C. The model drugs selected encompassed a wide variety of physicochemical properties in terms of crystallization tendency and potential for interaction with PEG. It was observed that compounds which crystallized rapidly and had weak interactions with PEG tended to be excluded from the interlamellar region of the PEG matrix. In contrast, drugs which had favorable interactions with PEG were incorporated into the interlamellar regions of the polymer up until the point at which the drug crystallized whereby phase separation occurred. These factors are likely to impact the effectiveness of drug/PEG systems as drug delivery systems.

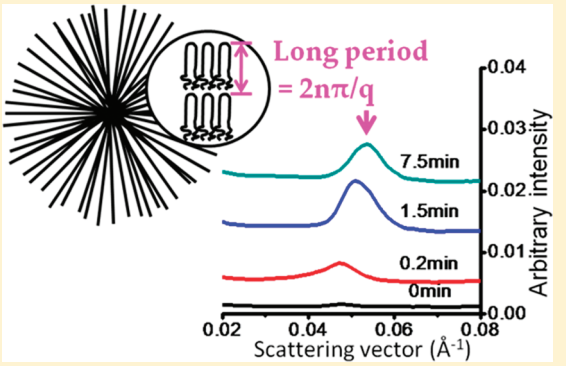

KEYWORDS: polyethylene glycol, structure, solid dispersion, solubility, interlamellar, interaction, small-angle X-ray scattering

INTRODUCTION

Polymers are widely used in drug delivery applications, in particular to control the release of the active pharmaceutical ingredient (API) from the matrix.[1,2] In addition, they can be used to improve the bioavailability of certain compounds by modification of the physical properties of the drug through forming solid dispersions. Solid dispersions, whereby the API is finely dispersed in a matrix, have received extensive attention as a potential approach to increase the bioavailability of poorly water-soluble compounds, a widespread issue with new APIs.[3−6] However, the poor reproducibility and inconsistent physicochemical properties during manufacturing, scale-up and storage, and the limited understanding of the mechanisms of dissolution enhancement have restricted the widespread application of this approach.[4−6] Both the physicochemical properties and the resultant dissolution behavior will be dependent on the microstructure of the solid dispersions. Solid dispersions are frequently prepared using highly water-soluble polymers as the matrix and polyethylene glycol (PEG)-based semicrystalline solid dispersions have attracted considerable interest due to the enhanced dissolution rates and bioavailability often see for these systems.[3,4] The microstructure of PEG-based solid dispersions is inherently complex due to the semicrystalline nature of the polymer, as well as the potentially variable crystallization behavior, location and domain size of the API.[7−9]

The solidification behavior of PEG in the presence of high molecular weight additives (i.e., other polymers) has been extensively probed using techniques such as small-angle X-ray scattering (SAXS) and differential scanning calorimetry (DSC).[9−13] From these studies it has been observed that, when a miscible amorphous component is added, the degree of exclusion of this component from the crystalline regions of PEG, i.e. exclusion into interlamellar, interfibrillar or interspherulitic regions, depends on the PEG crystallization rate, the mobility of the additive (determined by the blend T_g), and the presence or absence of any specific interactions between the two components. The inclusion/exclusion of the second component thus affects the microstructure of the blend. However, there are fewer studies investigating how the microstructure is altered in blends of PEG prepared with low molecular weight additives,[14−18] and the role of the aforementioned factors, known to be important for polymer blends, has not been elucidated.

In a previous study, the structure of PEG-based solid dispersions with different model APIs were probed after the API/PEG systems were solidified for 24 h.[18] The objective of the present study was to evaluate the evolution of the microstructure during the solidification process through the application of time-resolved small-angle X-ray scattering and wide-angle X-ray scattering (SAXS/WAXS) and to extend investigations to encompass a wider range of systems with a range of solubility in and miscibility with PEG. To achieve this, a range of model compounds with differing chemistry and physicochemical properties was selected.

Received: January 26, 2011
Accepted: March 31, 2011
Revised: March 23, 2011
Published: March 31, 2011

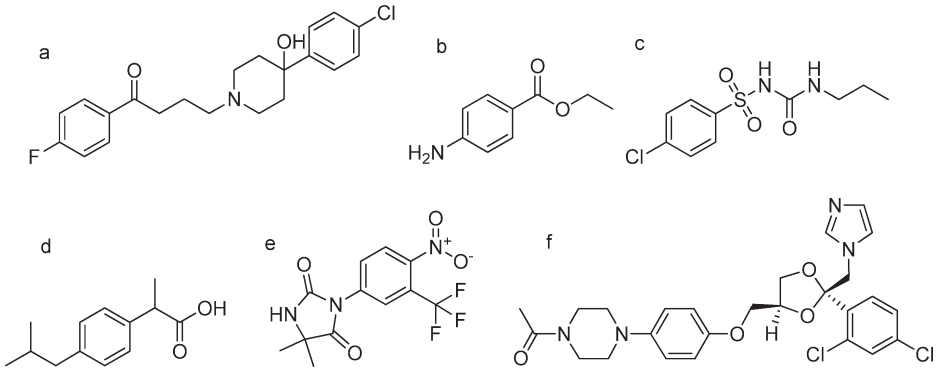

Figure 1. Chemical structures of (a) haloperidol, (b) benzocaine, (c) chlorpropamide, (d) ibuprofen, (e) nilutamide, and (f) ketoconazole.

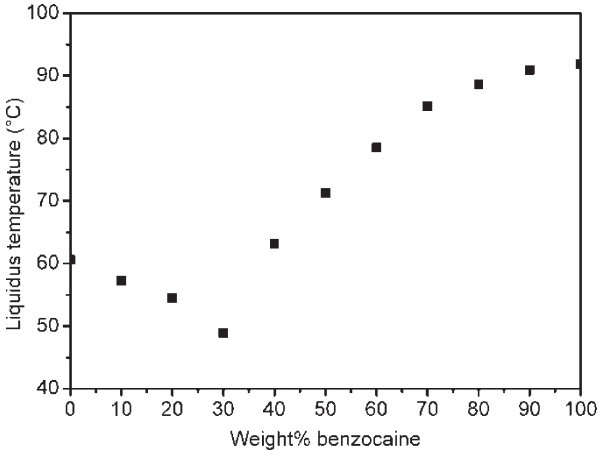

Figure 2. Phase diagram of BZC/PEG systems.

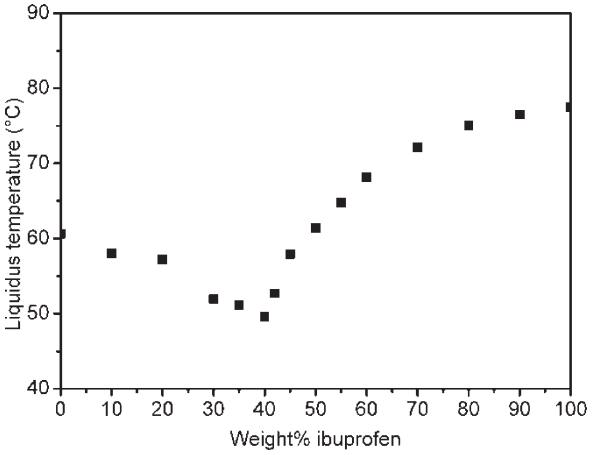

Figure 3. Phase diagram for IBP/PEG systems.

EXPERIMENTAL SECTION

Materials and Sample Preparation. Chlorpropamide (CPM), haloperidol (HLP), and nilutamide (NLU) were obtained from Sigma-Aldrich Inc. (St. Louis, Missouri). Benzocaine (BZC) was purchased from Spectrum Chemical (Gardena, CA). Ketoconazole (KET) was obtained commercially from Hawkins, Inc. (Minneapolis, MN). Ibuprofen (IBP) was purchased from Albemarle Co. (Baton Rouge, LA). PEG with a molecular weight 3350 was a kind gift from The Dow Chemical Company (Midland, MI). The structures of the model compounds are shown in Figure 1. Physical mixtures of the API and PEG were prepared by geometric mixing of a total of 1 g of powder, and dispersions were made by comelting the mixtures and allowing them to solidify at predetermined temperatures. Following solidification, the samples were stored in desiccators at low relative humidity.

Time-Resolved Simultaneous Small-Angle X-ray Scattering/Wide-Angle X-ray Scattering (SAXS/WAXS). The simultaneous SAXS/WAXS experiments were conducted at the Advanced Photon Source beam station 5-ID-D, Argonne National Lab. The simultaneous small and wide-angle scattering (SAXS/WAXS) instrument was equipped with a custom Roper charge coupled detector. The energy of the X-ray source was 17 keV ($\lambda = 0.73$ Å), and the distance of sample to SAXS and WAXS detectors was 3032 mm and 228 mm respectively. The q range for SAXS was 0.0085−0.23 $Å^{-1}$, and the range was 0.6−4.6 $Å^{-1}$ for WAXS. The SAXS range was calibrated using silver behenate (AgBeh), while the WAXS range was calibrated using lanthanum hexaboride (LaB_6) and the absolute intensity was calibrated using glassy carbon. Physical mixtures of the API and PEG (prepared as described above) were added to small aluminum pans (Tzero DSC sample pans, TA Instruments, New Castle, DE) and subjected to a temperature cycle using a Linkam DSC600 stage controlled by a Linkam CI-93 temperature programmer (Linkam Scientific Instruments Ltd., Surrey, U.K.). The sample was first heated to above the melting point of the API, followed by quench cooling to the specific solidification temperature.

Hot-Stage Microscopy. The API and PEG were physically mixed as described above and heated to the melting point of the API to form a homogeneous melt, followed by cooling to allow solidification. After storage for a few days (exact time depended on the crystallization rate of the API) at low relative humidity, the API/PEG solid dispersions were lightly ground using a mortar and pestle. The resultant powder was evaluated using a Nikon Eclipse E600 polarized light microscope (Nikon Inc., Melville, NY) equipped with a Linkam THMS 600 hot-stage (Linkam Scientific Instruments Ltd., Surrey, U.K.). The samples were heated at 1 °C/min until they were completely melted. The temperature where the last crystal melted was recorded and was used to construct the phase diagram.

Differential Scanning Calorimetry (DSC). Samples were analyzed using a TA Instruments Q2000 differential scanning

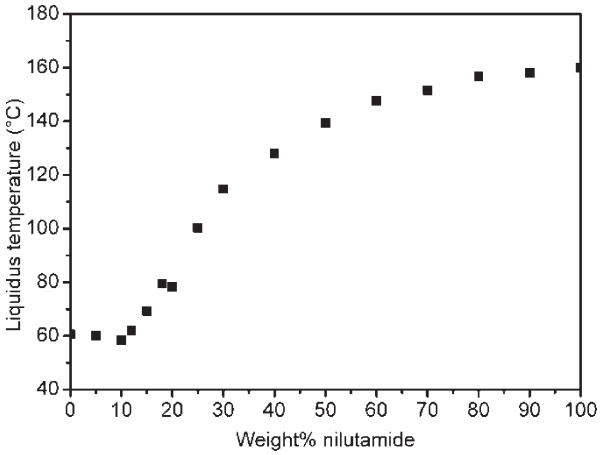

Figure 4. Phase diagram for NLU/PEG systems.

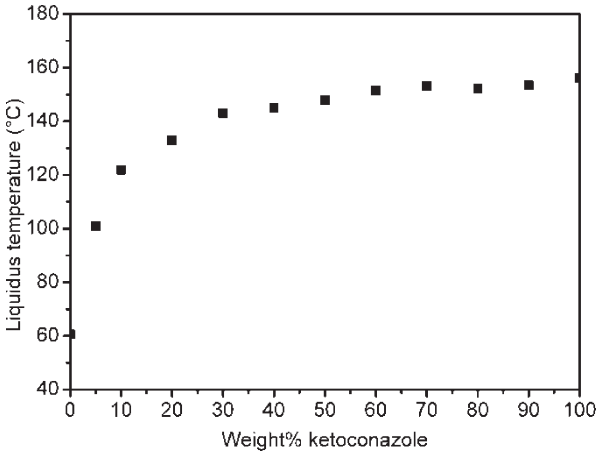

Figure 5. Phase diagram for KET/PEG systems.

calorimeter (TA Instruments, New Castle, DE, USA) with a nitrogen purge of 50 mL/min. The instrument was calibrated for temperature and enthalpy/cell constant by using indium (TA Instruments, New Castle, DE, USA). Samples were analyzed in sealed aluminum pans and were first equilibrated at 25 °C, followed by heating to above the melting point of the pure API at a rate of 1 °C/min. The DSC data were used to confirm the phase diagram constructed using hot-stage microscopy.

RESULTS AND DISCUSSION

Phase Diagrams of API/PEG Systems. Phase diagrams were constructed for the different API/PEG systems probed in this investigation (Figures 2−5) from optical microscopic determination of melting points, which were verified by DSC measurements (see Figure S1 in the Supporting Information). The phase diagrams of CPM/PEG and HLP/PEG systems have been previously constructed using an identical method, and the published results were used for these systems.[19] From Figures 2−5, it can be clearly seen that BZC/PEG, IBP/PEG and NLU/PEG systems showed eutectic formation, while KET/PEG is a monotectic system. The eutectic compositions for BZC/PEG, IBP/PEG and NLU/PEG are 30, 40 and 10% respectively and are determined by a combination of the melting point of the pure drug and the ability of the API to interact with PEG, as described previously.[19] CPM/PEG and HLP/PEG form eutectic and monotectic systems respectively whereby the CPM/PEG system has a eutectic composition of 35% and a minimum melting point of 55 °C.

Miscibility of API/PEG Systems. Interaction parameters for various API/PEG systems were calculated from the extent of melting point depression as a function of composition using the equation[20−23]

$$\left(\frac{1}{T_M^{mix}}-\frac{1}{T_M^{pure}}\right) = -\frac{R}{\Delta H_{fus}}\left[\ln \phi_{API} + \left(1-\frac{1}{m}\right)\phi_{polymer} + \chi\phi_{polymer}^{\ 2}\right] \quad (1)$$

where T_M^{mix} is the melting temperature of the API in the presence of the polymer, T_M^{pure} is the melting temperature of the API in the absence of the polymer, ΔH_{fus} is the heat of fusion of the pure API (values were taken from the literature[24]), m is the ratio of the molar volume of the polymer to that of the lattice site (defined here by the volume of the API), ϕ_{API} is the volume fraction of API, and $\phi_{polymer}$ is the volume fraction of PEG. The interaction parameter can be obtained from the slope of a plot of $-(\Delta H_{fus}/R)(1/T_M^{mix} - 1/T_M^{pure}) - \ln \phi_{API} - [1 - (1/m)]\phi_{polymer}$ vs $\phi_{polymer}^{\ 2}$. The calculated interaction parameters were normalized by multiplying the molar volume ratio of PEG to API and dividing by the number of chain segments in a single PEG molecule. The normalized interaction parameters for different API/PEG systems are listed in Table 1. More negative interaction parameters are consistent with a negative enthalpy of mixing between the drug and the polymer reflecting the formation of favorable drug−polymer interactions.

Estimation of API Solubility in PEG. It has been reported that the solubility of a small molecule additive in PEG can affect the microstructure of solidified PEG.[16] Therefore the solubility of the model APIs at 25 °C was estimated using the Van't Hoff equation (eq 2) as described previously.[18,25] Since this is below the melting point of PEG, the solubility estimate is for the supercooled liquid of PEG.

$$\frac{d \ln x}{dT} = \frac{\Delta H_f}{RT^2} \quad (2)$$

where x is the mole fraction solubility of the API in liquid PEG, ΔH_f is the heat of solution, R is the gas constant, and T is the temperature. To estimate the solubility at 25 °C, a plot of ln mole fraction solubility versus $1/T$ was constructed using the solubility values obtained from the phase diagrams shown in Figures 2−5. Linear regression analysis was used to fit the data, and the solubility at 25 °C was estimated by extrapolation. The estimated solubility of each API in PEG at 25 °C was converted to weight percent basis, and the values are listed in Table 1.

Table 1 shows that BZC, CPM and IBP have estimated solubility greater than 20% in PEG at 25 °C, consistent with the negative interaction parameters. Consideration of the chemical structure and physicochemical properties reveals the presence of hydrogen bond donors which can interact with the ether oxygen of PEG as well as moderate melting points. The formation of drug−polymer interactions for these systems was confirmed by FTIR spectroscopic analysis (see Figure S2 in the Supporting Information). NLU has a lower solubility in spite of the fact that it can form favorable interactions, which can be explained by the higher melting point. For KET and HLP, the interaction parameters are positive indicating that they have a

Table 1. Interaction Parameters and Solubility of API in PEG

API	interaction param[a]	solubility (% w/w) at 25 °C	eutectic composition	temp at eutectic composition (°C)
HLP[b]	0.08	0	monotectic	N/A
BZC	−0.23	28	30%	48.9
CPM[b]	−0.50	26	35%	55.0
IBP	−0.19	25	40%	49.6
NLU	−0.09	11	10%	58.4
KET	0.02	0	monotectic	N/A

[a] Calculated from melting point depression data with 50−80% API loading. [b] The results were calculated from the phase diagrams taken from the literature.[19]

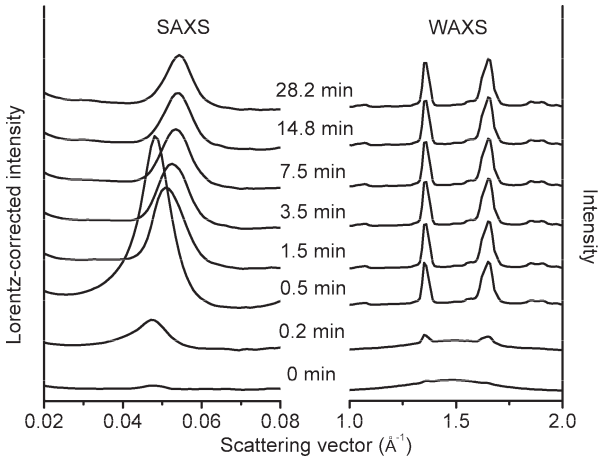

Figure 6. SAXS/WAXS of PEG crystallized at 25 °C.

lower degree of interaction with PEG, and consequently, they are almost insoluble in PEG at room temperature.

Evolution of PEG Microstructure. The structural evolution of PEG at different crystallization temperatures was studied using time-resolved SAXS/WAXS. Upon cooling molten PEG to 25 °C, crystallization occurred resulting initially in the formation of a nonintegral folded lamellar structure.[26,27] With time, the diffraction peak in the SAXS profile initially seen at $q \approx 0.047$ Å^{-1} shifted to a larger scattering vector as shown in Figure 6 (left section), while the two main characteristic peaks of the PEG crystal at $q \approx 1.36$ Å^{-1} and 1.65 Å^{-1} in the WAXS profile (Figure 6, right section) appeared immediately after solidification, and the position of the peaks was invariant during the crystallization process. Thus the initial long period value, L, was around 13.3 nm, and a decrease to 11.6 nm was observed within 30 min (Figure 7). After 24 h, L decreased further to 11.2 nm, and was constant thereafter. Lamella with a long period of 11.2 nm can be assigned to once-folded lamella.[26−29] When PEG was crystallized at 40 °C, the once-folded lamella was again the dominant structure. The long period initially increased slightly and then decreased to 12.6 nm after 40 min as shown in Figure 7. The long period was around 1 nm larger for PEG crystallized at 40 °C compared to PEG crystallized at 25 °C after 30 min of crystallization/solidification, but after 24 h, L was virtually identical (11.2 nm) for the two crystallization temperatures.

Evolution of Microstructure in the API/PEG Solid Dispersions. The microstructure of PEG following solidification with different model APIs was also evaluated using time-resolved SAXS/WAXS. As

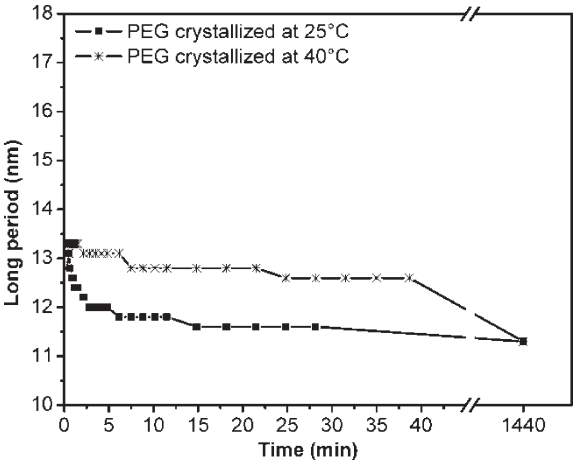

Figure 7. Long period for once-folded PEG lamella evolved at 25 and 40 °C.

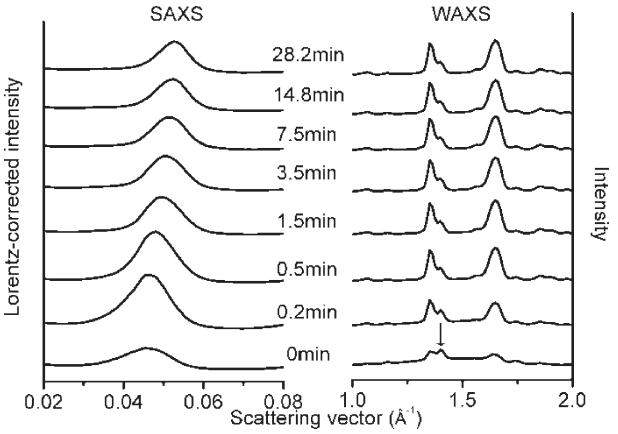

Figure 8. SAXS/WAXS of HLP/PEG (20/80) crystallized at 25 °C.

described above, the various model APIs have different estimated solubilities in supercooled liquid PEG, as well as a range of interaction parameters, reflecting their differing ability to interact with PEG. Furthermore, it was also observed that the APIs exhibited varying crystallization tendencies, both as pure compounds and following comelting with PEG, a property of likely relevance in determining their effect on the resultant microstructure. Thus the phase behavior of each pure API and PEG following melting and cooling to room temperature was determined using polarized light microscopy. HLP, BZC and PEG were observed to crystallize immediately following cooling to room temperature. CPM, NLU and IBP crystallized within a few hours, while KET was amorphous after cooling and had not crystallized after a 24 h storage period at room temperature. In addition, the various APIs have different glass transition temperatures: NLU and KET have glass transition temperatures above 25 °C, while the glass transition temperatures for the other APIs are below 25 °C.[24]

HLP/PEG Dispersions (Rapidly Crystallizing API, Low Solubility). HLP has weak interactions with PEG, and the solubility is estimated to be low (Table 1). The API crystallized very fast upon cooling from the melt in the absence of PEG. When the HLP/PEG system was solidified at 25 °C, the WAXS data (Figure 8, right section) indicated that HLP crystallized immediately after solidification as demonstrated by the presence of a

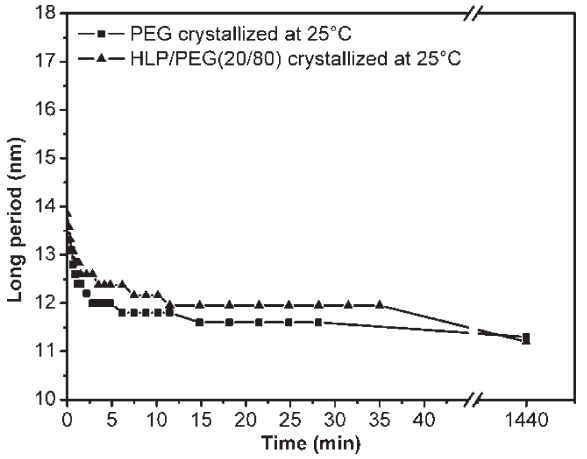

Figure 9. Long period evolution for once-folded PEG lamella in the HLP/PEG (20/80) dispersion at 25 °C.

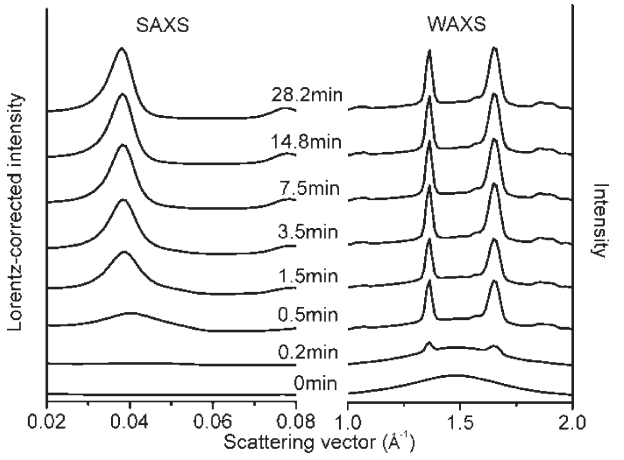

Figure 10. SAXS/WAXS of BZC/PEG (20/80) crystallized at 25 °C.

characteristic peak ($q \approx 1.40$ Å^{-1}, indicated by the arrow in Figure 8) for crystalline HLP. From Figure 9, it is evident that the evolution of the long period for the PEG once-folded lamella in the presence of HLP is essentially the same as that observed in the absence of the API. The L for PEG lamella in the HLP/PEG dispersion was initially slightly larger, however, after 24 h there was essentially no difference in the value, which was around 11.2 nm. The lack of influence of HLP on the crystallization of PEG most likely results from its rapid removal from the PEG phase due to the fast crystallization of the API on cooling.

BZC/PEG Dispersions (Rapidly Crystallizing API, High Solubility). Pure BZC displays rapid crystallization at room temperature upon cooling of the pure drug melt. However, different from HLP, BZC has stronger interactions with and a higher solubility in PEG. For these samples, time-resolved SAXS/WAXS data were collected for 30 min, and followed by another measurement after 24 h. Over the 30 min time period, diffraction peaks arising from crystalline BZC were absent in the WAXS data (Figure 10), indicating that BZC failed to crystallize over this time frame. The crystallization rate of BZC has thus been reduced by the addition of PEG, most likely due to the lower extent of supercooling experienced by the API (see Figure 2, the melting point of the 20/80 dispersion is 55 °C compared to 92 °C for pure

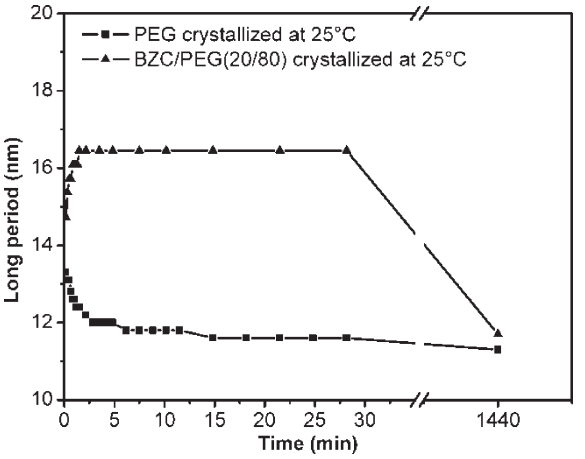

Figure 11. Long period evolution for once-folded PEG lamella in the BZC/PEG (20/80) dispersion at 25 °C.

benzocaine). Furthermore, the corresponding SAXS results (Figure 10 and Figure 11) show that the long period was much larger in the BZC/PEG (20/80) dispersions solidified at 25 °C relative to that found in pure PEG at the same time point during the solidification process. The increase of L for PEG in the BZC/PEG system could conceivably result either from the decreased degree of supercooling of PEG due to the melting point depression caused by the presence of BZC (see Figure 2) or from the incorporation of BZC in PEG lamella. Given the relatively small effect of changing the degree of supercooling on the value of the long period at short solidification times (see data for PEG crystallized at 25 and 40 °C shown in Figure 7 where the difference in L is around 1 nm after 30 min), the former explanation is unlikely to account for the large change seen in L. Therefore, the 4−5 nm increase of L can be largely attributed to the incorporation of BZC in the interlamellar region of PEG. With extended periods of time (24 h), BZC crystallized and was expelled from the interlamellar region of PEG resulting in a decrease in L from 16.5 nm to 11.4 nm, close to the value found for pure PEG.

CPM/PEG Dispersions (Intermediate Crystallizing API, High Solubility, T_g < 25 °C). Pure CPM crystallizes at an intermediate rate upon cooling from the melt, remaining amorphous for a few hours when kept at room temperature. This compound is also able to form strong interactions with PEG based on the value of the interaction parameter (Table 1) and also has a high solubility in PEG. When the CPM/PEG system was solidified at 25 °C, the L was more than 3 nm larger in the dispersion than observed for pure PEG at a comparable solidification time (after approximately 28 min), suggesting interlamellar incorporation of CPM in PEG (Figure 12). The WAXS data (data not shown) indicated that CPM did not undergo crystallization over this time frame. However, after a 24 h storage period, most of CPM appeared to have crystallized based on the WAXS results and the phase separation of CPM resulted in a corresponding decrease in the long period for PEG (Figure 12), as observed for BZC.

IBP/PEG Dispersions (Intermediate Crystallizing API, High Solubility, T_g < 25 °C). IBP initially remains amorphous on cooling the pure melt to room temperature, and crystallization is observed after a few hours. IBP also forms strong interactions with PEG (Table 1). During the evolution of L in the IBP/PEG (20/80) systems at 25 °C, the long period first increased, and stayed constant for about 100 min, followed by a decrease in

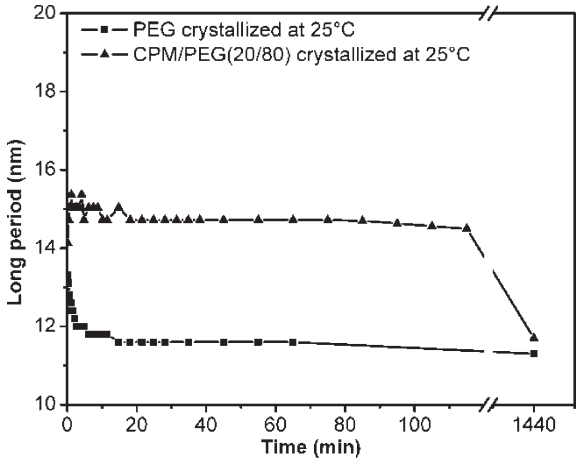

Figure 12. Long period evolution for once-folded PEG lamella in the CPM/PEG (20/80) dispersion at 25 °C.

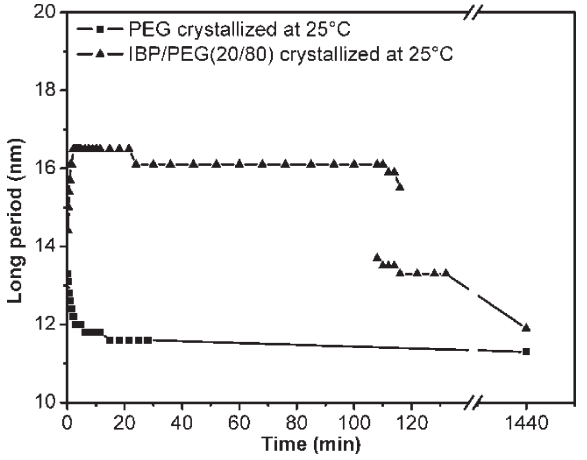

Figure 13. Long period evolution for once-folded PEG lamella in the IBP/PEG (20/80) dispersion at 25 °C. (The two long period values between 100 min and 120 min correspond to two diffraction peaks observed in the SAXS data, see Figure 14.)

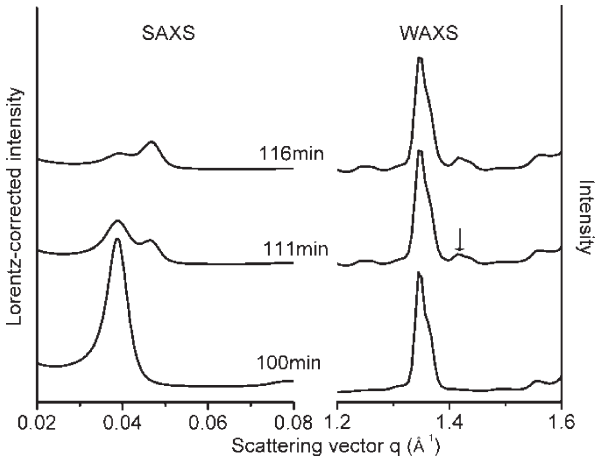

Figure 14. SAXS/WAXS of IBP/PEG (20/80) crystallized at 25 °C.

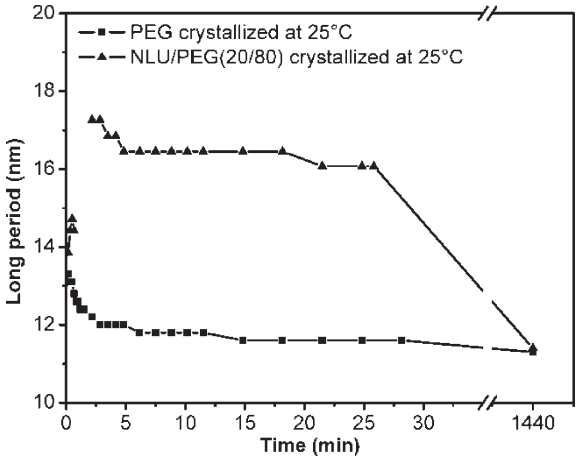

Figure 15. Long period evolution for once-folded PEG lamella in the NLU/PEG (20/80) dispersion at 25 °C.

value. The long period was 4.9 nm larger in the IBP/PEG (20/80) dispersion than that in pure PEG after 20 min solidification at 25 °C. After approximately 100 min, the long period underwent a sudden decrease to 13.2 nm over a period of a few minutes (Figure 13). From the SAXS/WAXS profiles (Figure 14), it was observed that this sudden decrease in long period corresponded to the crystallization of IBP. Hence, at t = 100 min, IBP was still amorphous and there was a diffraction peak from PEG lamella in SAXS at around $q \approx 0.039$ Å^{-1} whereas, at t = 111 min, a new peak evolved at $q \approx 0.047$ Å^{-1} in the SAXS pattern, and a characteristic peak for crystalline IBP could be detected in the WAXS data (denoted by the arrow in Figure 14). As the crystallization time increased to 116 min, the peak at $q \approx 0.047$ Å^{-1} in SAXS became the dominant peak. Consistent with the systems discussed above, crystallization of the drug results in its exclusion from the interlamellar regions of PEG and hence a decrease in the value of the long period.

NLU/PEG Dispersions (Intermediate Crystallizing API, Moderate Solubility, T_g > 25 °C). The model APIs discussed above all have glass transition temperatures below 25 °C, lower than the solidification temperature of 25 °C. To evaluate the importance of T_g, it is also of interest to investigate the structural evolution in API/PEG systems containing APIs that have glass transitions above 25 °C. The glass transition of NLU is around 33 °C, the solubility in PEG is moderate and NLU has an intermediate crystallization tendency whereby no crystallization is seen immediately upon cooling to room temperature from the melt. As shown in Figure 15, for the NLU/PEG (20/80) dispersion solidified at 25 °C, L first increased, and then remained relatively constant for a period of 30 min at a value of around 16 nm. After 24 h, the WAXS data indicated that NLU had crystallized with a corresponding decrease in the long period, once again indicating removal of the API from the interlamellar region of PEG; the long period was virtually the same as observed for pure PEG. Thus in this case, the higher T_g of the compound did not appear to impact the behavior in a manner different from that seen for the lower T_g compounds discussed above.

KET/PEG Dispersions (Slowly Crystallizing API, Low Solubility, T_g > 25 °C). KET has weak interaction with and low solubility in PEG. The glass transition for the API is 44 °C and the drug fails to crystallize on cooling from the melt, even after 24 h. When KET/PEG is solidified at 25 °C, the L evolution was almost the same as for pure PEG hence KET has almost no effect on the

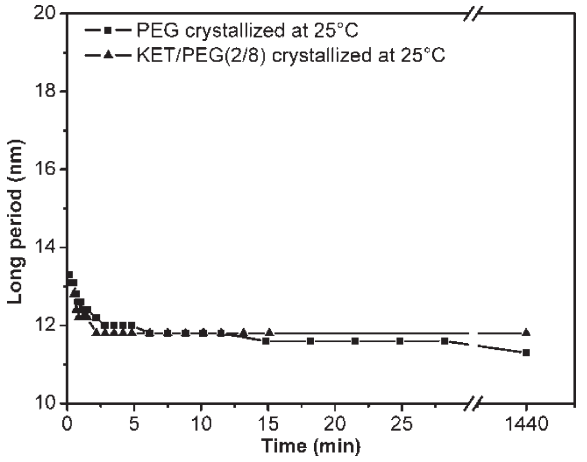

Figure 16. Long period evolution for once-folded PEG lamella in the KET/PEG (20/80) dispersion at 25 °C.

Table 2. Value of Long Period of PEG Matrix and Crystallinity of the API in API/PEG Systems

API	long period of PEG at 30 min	API phase behavior at 30 min	long period of PEG at 24 h	API phase behavior at 24 h
HLP	12.0	crystalline	11.2	crystalline
BZC	16.5	amorphous	11.4	partially crystalline
CPM	14.7	amorphous	11.7	partially crystalline
IBP	16.1	amorphous	11.9	partially crystalline
NLU	16.0	amorphous	11.4	partially crystalline
KET	11.8	amorphous	11.8	amorphous

lamellar structure of PEG (Figure 16). This is likely due to the positive interaction parameter of KET with PEG, which may indicate a low tendency to mix with PEG and result in a large extent of exclusion from the interlamellar region. The WAXS data showed that no crystallization of KET had occurred after 24 h. Clearly, for this system, the higher T_g of the API did not prevent the phase separation of the compound.

Table 2 summarizes the size of the PEG long period in the presence of different APIs at 30 min and 24 h post solidification. It can be clearly seen that in the presence of APIs that can interact with PEG (BZC, CPM, IBP or NLU, see Table 1) the long period is much larger than for the non-interacting APIs (KET) for time frames where the API has not yet crystallized. This suggests that interlamellar incorporation is favored for molecules that can interact strongly with PEG. However, the crystallization tendency of the small molecule also has to be considered; upon crystallization, the API is removed from the interlamellar region, resulting in a concurrent decrease in the long period. For APIs that interact weakly with PEG, in particular KET, even though no API crystallization was seen after 24 h, the small molecule has little discernible impact on the lamellar structure of PEG.

CONCLUSIONS

The addition of a small organic molecule to PEG can result in structural modifications to the polymer in the form of changes to the long period (L) following solidification of a molten blend. The location of the API could thus be inferred from the change of long period (L) of PEG whereby APIs having a higher solubility in and strong interaction with PEG resulted in the larger increase of long period compared to weakly interacting APIs. The evolution of the long period was dramatically affected by the crystallization behavior of the API such that crystallization of the small molecule led to a marked decrease in the long period. Combined SAXS/WAXS time-resolved studies were found to be extremely useful for understanding the effect of API phase behavior on PEG structure, and the results of this study help explain the often noted variability in the physicochemical properties of drug/PEG dispersions as a function of storage time.

ASSOCIATED CONTENT

Supporting Information. DSC data and FTIR spectrum. This material is available free of charge via the Internet at http://pubs.acs.org.

AUTHOR INFORMATION

Corresponding Author

*Purdue University, Department of Industrial and Physical Pharmacy, 575 Stadium Mall Drive, West Lafayette, IN 47907. E-mail: lstaylor@purdue.edu. Tel: +1-765-496-6614. Fax: +1- 765-494-6545.

ACKNOWLEDGMENT

Portions of this work were performed at the DuPont-Northwestern-Dow Collaborative Access Team (DND-CAT) located at Sector 5 of the Advanced Photon Source (APS). DND-CAT is supported by E.I. DuPont de Nemours & Co., The Dow Chemical Company and the State of Illinois. Use of the APS was supported by the U.S. Department of Energy, Office of Science, Office of Basic Energy Sciences, under Contract No. DE-AC02-06CH11357. We acknowledge the National Science Foundation Engineering Research Center for Structured Organic Particulate Systems (NSF ERC-SOPS) (EEC-0540855) for financial support.

REFERENCES

(1) Uhrich, K. E.; Cannizzaro, S. M.; Langer, R. S. Polymeric systems for controlled drug release. *Chem. Rev.* **1999**, *99*, 3181–3198.

(2) Langer, R.; Peppas, N. A. Advances in biomaterials, drug delivery, and bionanotechnology. *AIChE J.* **2003**, *49* (12), 2990–3006.

(3) Leuner, C.; Dressman, J. Improving drug solubility for oral delivery using solid dispersions. *Eur. J. Pharm. Biopharm.* **2000**, *50*, 47–60.

(4) Chiou, W. L.; Riegelman, S. Pharmaceutical applications of solid dispersion systems. *J. Pharm. Sci.* **1971**, *60*, 1281–1302.

(5) Serajuddin, A. T. M. Solid dispersion of poorly water-soluble drugs: early promises, subsequent problems, and recent breakthroughs. *J. Pharm. Sci.* **1999**, *88*, 1058–1066.

(6) Craig, D. Q. M. The mechanisms of drug release from solid dispersions in water-soluble polymers. *Int. J. Pharm.* **2002**, *231*, 131–144.

(7) Dordunoo, S. K.; Ford, J. L.; Rubinstein, M. H. Preformulation studies on solid dispersions containing triamterene or temazepam in polyethylene glycols or gelucire 44/14 for liquid filling of hard gelatin capsules. *Drug Dev. Ind. Pharm.* **1991**, *17* (12), 1685–1713.

(8) Ginés, J. M.; Arias, M. J.; Moyano, J. R.; Sánchez-Soto, P. J. Thermal investigation of crystallization of polyethylene glycols in solid dispersions containing oxazepam. *Int. J. Pharm.* **1996**, *143*, 247–253.

(9) Talibuddin, S.; Wu, L.; Runt, J. Microstructure of melt-miscible, semicrystalline polymer blends. *Macromolecules* **1996**, *29*, 7527–7535.

(10) Silvestre, C.; Karasz, F. E.; Macknight, W. J.; Martuscelli, E. Morphology of poly(ethylene oxide)/poly(vinyl acetate) blends. *Eur. Polym. J.* **1987**, *23*, 745–751.

(11) Silvestre, C.; Cimmino, S.; Martuscelli, E. Poly(ethylene oxide)/poly(methyl methacrylate) blends: influence of tacticity of poly(methyl methacrylate) on blend structure and miscibility. *Polymer* **1987**, *28*, 1190–1199.

(12) Russell, T. P.; Ito, H. Neutron and X-ray scattering studies on semicrystalline polymer blends. *Macromolecules* **1988**, *21*, 1703–1709.

(13) Utracki, L. A. *Polymer Blends Handbook*, 1st ed.; Kluwer Academic Publishers: Dordrecht, The Netherlands, 2002; pp 203−212.

(14) Mahlin, D.; Ridell, A.; Frenning, G. Solid-state characterization of PEG4000/monoolein mixtures. *Macromolecules* **2004**, *37*, 2665–2667.

(15) Qian, F.; Tao, J.; Desikan, S.; Hussain, M.; Smith, R. L. Mechanistic investigation of Pluronic based nano-crystalline drug-polymer solid dispersions. *Pharm. Res.* **2007**, *24*, 1551–1560.

(16) Unga, J.; Tajarobi, F.; Norder, O.; Frenning, G.; Larsson, A. Relating solubility data of parabens in liquid PEG 400 to the behavior of PEG 4000-parabens solid dispersions. *Eur. J. Pharm. Biopharm.* **2009**, *73*, 260–268.

(17) Unga, J.; Matsson, P; Mahlin, D. Understanding polymer-lipid solid dispersions-the properties of incorporated lipids govern the crystallization behavior of PEG. *Int. J. Pharm.* **2010**, *386*, 61–70.

(18) Zhu, Q.; Taylor, L. S.; Harris, M. T. Evaluation of the microstructure of semicrystalline solid dispersions. *Mol. Pharmaceutics* **2010**, *7* (4), 1291–1300.

(19) Baird, J. A.; Taylor, L. S. Evaluation and modeling of the eutectic composition of various drug-polyethylene glycol solid dispersions. *Pharm. Dev. Technol.* **2010**, DOI: 10.3109/10837450903584936.

(20) Flory, P. J. *Principles of Polymer Chemistry*; Cornell University Press: Ithaca, NY, 1953; p 549.

(21) Nishi, T.; Wang, T. T. Melting point depression and kinetic effects of cooling on crystallization in poly(viny1idene fluoride)-poly(methyl methacrylate) mixtures. *Macromolecules* **1975**, *8* (6), 909–915.

(22) Hoei, Y.; Yamaura, K.; Matsuzawa, S. A lattice treatment of crystalline solvent-amorphous polymer mixtures on melting point depression. *J. Phys. Chem.* **1992**, *96*, 10584–10586.

(23) Marsac, P. J.; Shamblin, S. L.; Taylor, L. S. Theoretical and practical approaches for prediction of drug-polymer miscibility and solubility. *Pharm. Res.* **2006**, *23* (10), 2417–2426.

(24) Baird, J. A.; Eerdenbrugh, B. V.; Taylor, L. S. A classification system to assess the crystallization tendency of organic molecules from undercooled melts. *J. Pharm. Sci.* **2010**, *99* (10), 3787–3806.

(25) Connors, K. A. 2002. *Thermodynamics of Pharmaceutical Systems - An Introduction for Students of Pharmacy*; Wiley-Interscience: Hoboken, NJ, 2002; pp 118−119.

(26) Cheng, S. Z. D.; Zhang, A. Q.; Chen, J. H.; Heberer, D. P. Nonintegral and integral folding crystal growth in low-molecular mass poly(ethylene oxide) fractions. I. Isothermal lamellar thickening and thinning. *J. Polym. Sci., Part B: Polym. Phys.* **1991**, *29*, 287–297.

(27) Cheng, S. Z. D.; Chen, J. H.; Zhang, A. Q.; Barley, J. S. Isothermal thickening and thinning processes in low molecular weight poly(ethylene oxide) fractions crystallized from the melt: 2.Crystals involving more than one fold. *Polymer* **1992**, *33* (6), 1140–1149.

(28) Arlie, P. J. P.; Spegt, P.; Skoulios, A. Etude de la cristallisation des polymères II. Structure lamellaire et repliement des chaînes du polyoxyéthylène. *Macromol. Chem. Phys.* **1967**, *104*, 212–229.

(29) Buckley, C. P.; Kovacs, A. J. Melting behavior of low molecular weight poly(ethylene-oxide) fractions 2. Folded chain crystals. *Colloid Polym. Sci.* **1976**, *254* (8), 695–715.